J Fluoresc (2011) 21:813–823
DOI 10.1007/s10895-010-0775-1

ORIGINAL PAPER

Synthesis, Crystal Structure, Interaction with BSA and Antibacterial Activity of La(III) and Sm(III) Complexes with Enrofloxacin

Yan-Jun Wang · Rui-Ding Hu · Dong-Hua Jiang · Ping-Hua Zhang · Qiu-Yue Lin · Yun-Yun Wang

Received: 25 August 2010 / Accepted: 16 November 2010 / Published online: 3 December 2010

Abstract Two new La(III) and Sm(III) complexes with enrofloxacin (HER, 1-cyclopropyl-7-(4-ethyl-1-piperazinyl)-6-fluoro-1,4-dihydro-4-oxo-3-quinoline carboxylic acid, $C_{19}H_{21}FN_3O_3$), $[La_2(ER)_6(H_2O)_2]\cdot 14H_2O$(**1**) and $[Sm_2(ER)_6(H_2O)_2]\cdot 14H_2O$(**2**) have been synthesized and characterized by elemental analysis, FT-IR, TG-DTG and X-ray single crystal diffraction. Both of the complexes are triclinic system with space group $P\bar{1}$. The structure of the complexes show that each rare earth atom in both complexes was nine-coordinated. Two of the enrofloxacin ions acted as tridentate chelate and bridging ligands, while the others as bidentate chelate ligands. The binding reaction between the complexes and bovine serum albumin (BSA) was studied by UV-vis absorption spectra and fluorescence spectroscopy. The results indicated that the two complexes had a quite strong ability to quench the fluorescence from BSA and the binding reaction was mainly a static quenching process. The binding constants $K_A/(L\cdot mol^{-1})$ were 1.46×10^5(**1**) and 8.59×10^6(**2**) and one binding site was formed. The synchronous spectroscopy suggested that tryptophan residues were placed in BSA. It was also found that the two complexes exhibited greater antimicrobial activity than enrofloxacin at given concentrations.

Keywords Enrofloxacin · Rare earth complexes · Crystal structure · Interaction with BSA · Antibacterial activity

Y.-J. Wang · R.-D. Hu · Q.-Y. Lin
Zhejiang Key Laboratory for Reaction Chemistry on Solid Surfaces, Jinhua 321004, China

Y.-J. Wang · D.-H. Jiang · P.-H. Zhang · Q.-Y. Lin (✉) · Y.-Y. Wang
College of Chemical and Life Science, Zhejiang Normal University, Jinhua 321004, China
e-mail: sky51@zjnu.cn

Introduction

Protein plays an important role in the life activities of cells and organisms. Plasma albumin has many physiological functions, for example, depoting and transporting endogenous and exogenous compounds [1, 2]. The interaction between protein and drug molecules resulted in the formation of a stable protein-drug complex which could influence absorption, distribution, metabolism and excretion properties of typical drugs [3].

Enrofloxacin [HER, 1-cyclopropyl-7-(4-ethyl-1-piperazinyl)-6-fluoro-1,4-dihydro-4-oxo-3-quinoline carboxylic acid] (Fig. 1), the third-generation fluoroquinolone antibacterial agent, has wide antimicrobial spectrum and strong antibacterial activity [4]. It was mainly used to treat urinary tract, respiratory tract and skin infectious diseases [5–7]. As a typical quinoline, it could coordinate to metal ions as chelates through ring carbonyl and carboxylate oxygen atoms [8, 9].

In recent years, rare earth metal ions and their compounds were paid extensive attention to because of their significant anti-inflammatory, antibacterium, and other biological activities [10, 11]. As functional metal centers, rare earth metals have been widely used for their fantastic coordination properties and special chemical charactertics arising from 4f electrons and the properties to form isostructural complexes [12]. Thus, we focused on the study of rare earth metal (III) complexes with enrofloxacin and investigated their antibacterial activity.

In this paper, the La (III) and Sm (III) complexes were synthesized and characterized by elemental analysis, FT-IR, TG-DTG and X-ray single crystal diffraction. The interaction between two complexes and BSA was investigated by UV-vis spectra and fluorescence spectra. The quenching mechanisms were also studied and discussed.

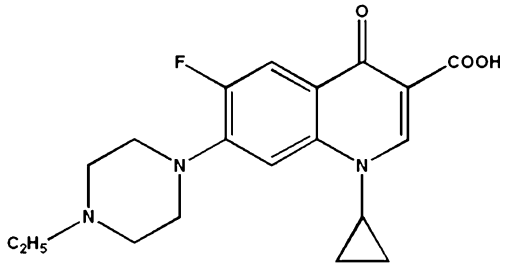

Fig. 1 The structure of enrofloxacin (HER)

Experimental

Reagents and Instruments

All chemicals were obtained commercially and used without further purification. Ln_2O_3 (Ln=La, Sm) (A.R.) was purchased from Sinopharm Chemical Reagent Co., LtdS. Enrofloxacin (A.R.) was obtained from Wuhan Yuancheng Technology Development Co., Ltd. Tris-(hydroxymethyl)aminomethane (Tris, A.R.) and bovine serum albumin (BSA) were purchased from Shanghai Bio Life Science and Technology Co., Ltd. The solvents were all of analytic grade. Doubly distilled water was used to prepare buffer solutions. Crystallographic data were collected on a Bruker APEX II diffractometer. Elemental analyses of C, H and N were carried out in a Vario EL III elemental analyzer. Infrared spectra were recorded as KBr pellet by using a NEXUS-670 FT-IR spectrometer. The thermal behavior was monitored on a TGA/SDTA851^e thermo gravimetric and differential thermal analyzer. UV-vis spectra were recorded on a UV-2501PC spectrophotometer. Fluorescence emission spectra were recorded with a Perkin-Elermer LS-55 spectrofluorometer.

Synthesis of the Complexes

$[La_2(ER)_6(H_2O)_2]\cdot 14H_2O$ (**1**)

A mixture of 0.15 mmol La_2O_3, 0.15 mmol Enrofloxacin (HER, $C_{19}H_{22}FN_3O_3$) and 10 mL distilled water was sealed in a 25 mL Teflon-lined stainless vessel and heated at 453 K for 3d, then cooled slowly to room temperature. The solution was filtered and block yellow single crystals were obtained. Calc(%). for $C_{114}H_{158}F_6N_{18}O_{34}La_2$: C, 50.41; H, 5.86; N, 9.28. Found(%): C, 50.47; H, 5.10; N, 9.26.

Table 1 Crystallographic data and structural refinements for complexes **1** and **2**

Compound	**1**	**2**
Empirical formula	$C_{114}H_{158}F_6La_2N_{18}O_{34}$	$C_{114}H_{158}F_6Sm_2N_{18}O_{34}$
Formula weight	2716.40	2716.40
Crystal size / (mm)	0.217×0.105×0.060	0.286×0.148×0.106
Temperature / (K)	296(2)	296(2)
Crystal system	Triclinic	Triclinic
Space group	$P\bar{1}$	$P\bar{1}$
a / (Å)	14.9165(19)	14.9165(19)
b / (Å)	14.999(2)	14.999(2)
c / (Å)	18.086(2)	18.086(2)
α / (°)	69.821(9)	69.821(9)
β / (°)	80.441(9)	80.441(9)
γ / (°)	63.108(8)	63.108(8)
V / (Å^3)	3387.1(7)	3387.1(7)
Z	1	1
Dc / (g·cm^{-3})	1.332	1.332
F(000)	1408	1408
θ range / (°)	1.20≤θ≤25.00	1.20≤θ≤25.00
Limiting indices	−17≤h≤17, −17≤k≤17, −21≤l≤21	−17≤h≤17, −17≤k≤17, −21≤l≤21
Reflections collected/unique	44245 / 11889	44745 / 11917
Observed reflections [$I>2\sigma(I)$]	7409	9396
Goodness of fit on F^2	1.004	1.058
Final R indices [$I>2\sigma(I)$]	R=0.0720, wR=0.2009	R=0.0622, wR=0.1816
R indices (all data)	R=0.1187, wR=0.2259	R=0.0792, wR=0.1983
$\Delta\rho_{max}$, $\Delta\rho_{min}$ / (e·Å^{-3})	1.195, −0.614	1.004, −0.825

Table 2 Characteristic absorptions (cm^{-1}) of IR spectra

	ν(O-H)	$\nu_{as}(COO^-)$	$\nu_s(COO^-)$	$\Delta\nu$[a]	ν(C=O)	ν(Ln-O)
Enrofloxacin	3431(w)	1734(vs)	1734(vs)	–	1627(vs)	–
$[La_2(ER)_6(H_2O)_2]\cdot 14H_2O$ (**1**)	3422(s)	1577(vs), 1529(s), 1485(vs)	1380(s)	197, 149, 105	1618(vs)	496(w)
$[Sm_2(ER)_6(H_2O)_2]\cdot 14H_2O$ (**2**)	3419(s)	1576(vs), 1529(s), 1484(vs)	1378(s)	198, 151, 104	1619(vs)	501(w)

[a] $\Delta\nu=\nu_{as}(COO^-)-\nu_s(COO^-)$

*$[Sm_2(ER)_6(H_2O)_2]\cdot 14H_2O$ (**2**)*

A mixture of 0.05 mmol Sm_2O_3, 0.2 mmol Enrofloxacin and 10 mL distilled water was sealed in a 25 mL Teflon-lined stainless vessel and heated at 453 K for 3d, then cooled slowly to room temperature. The solution was filtered and block yellow single crystals were obtained. Calc(%). for $C_{114}H_{158}F_6N_{18}O_{34}Sm_2$: C, 50.65; H, 5.74; N, 9.33. Found(%): C, 51.21; H, 5.16; N, 9.04.

X-ray Crystallography

Single crystals were used for X-ray diffraction analysis. Data collections were performed with MoK_α radiation (λ=0.71073 Å) on a Bruker APEX II diffractometer at 296 (2) K. The intensity data were corrected by Lorentz-polarization factors and empirical absorption. The crystal structures were solved by means of direct methods and expanded with difference Fourier techniques. All non-hydrogen atoms were refined anisotropically. Except the hydrogen atoms on oxygen atoms were located from the difference Fourier maps, the other hydrogen atoms were generated geometrically. All calculations were performed by full-matrix least-squares with the SHELXTL-97 program package [13, 14]. Crystallographic data of **1** and **2** were given in Table 1.

Interaction with BSA

BSA stock solutions (7.46 μmol·L^{-1} in 0.05 mol·L^{-1} NaCl) were stored at 4 °C. Two complexes were dissolved in DMSO. Tris-HCl buffer (pH 7.4) was prepared in 50 mmol·L^{-1} NaCl / 5 mmol·L^{-1} Tris-HCl.

UV-vis Absorption Spectra

The reaction of complex with BSA was carried out by successive addition of the 0.1 mmol·L^{-1} complex solution (0–0.13 mL) to a fixed amount of BSA (a final concentration of 4.48 μmol·L^{-1}) in each test tube. The mixture was diluted to 5.00 mL with Tris-HCl buffer. Absorption spectra measurements were carried out at 230–400 nm and complex in Tris-HCl buffer was used as reference.

Fluorescence Spectra

A quantitative analysis of the potential interaction between complexes and BSA was performed by fluoremetric titration. The reaction was carried out by mixing 0.20 mL BSA solution with 2.80 mL Tris-HCl buffer, and the range of the 0.10 mmol·L^{-1} complex solution was gradually titrated into the cell. The accumulated volumes were 2.5, 5.0, 7.5, 10.0, 12.5, 15.0, 17.5, 20.0μL, respectively. Fluorescence quenching spectra were obtained at excitation (280 nm) and emission (280–520 nm).

Synchronous Fluorescence Spectra

Synchronous fluorescence spectra were scanned on the same condition in Section 2.3.2. The spectra were measured at two different $\Delta\lambda$ ($\Delta\lambda=\lambda_{em}-\lambda_{ex}$) values, 15 nm and 60 nm.

Antibacterial Assay

Gram-positive (*Bacillus subtilis, Staphylococcus aureus*) and Gram-negative (*Escherichia coli*) bacteria were selected as antibacterial assay *in vitro*. The tested compounds were dissolved in DMSO. Beef-protein medium and the Oxford cups were placed at 121 °C for 30 min. The mediums were poured into culture dishes to form solid plates. A standard inoculum (10^5c.f.u/mL) was introduced onto the surface of

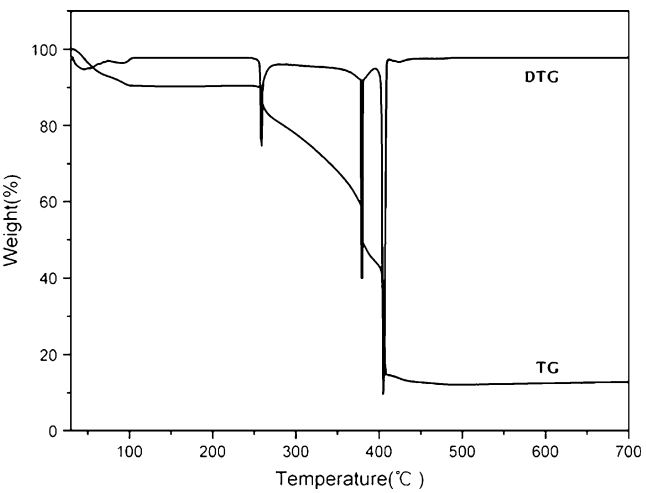

Fig. 2 TG-DTG curve of complex **1**

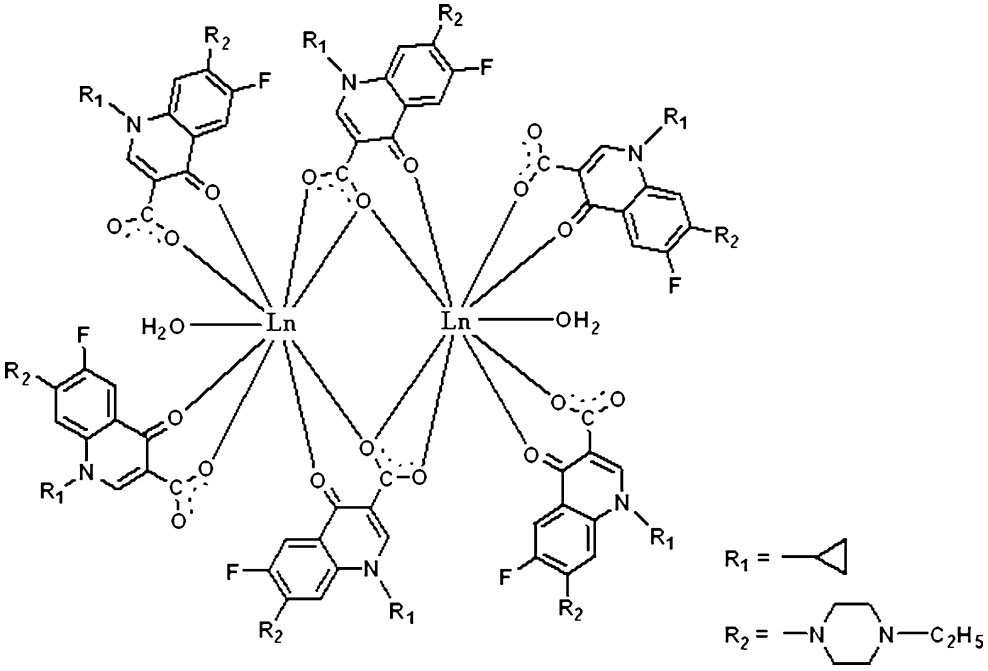

Fig. 3 The coordination model of the complexes (Ln(III)=La (III), Sm (III))

sterile agar plates and distributed evenly. The Oxford cups, previously soaked in a known concentration of the test compounds, were placed in beef-protein medium. The culture dishes were incubated at 36±1 °C. After 24 h diameters of antibacterial active rings were assayed.

Results and Discussion

Infrared Spectra

Characteristic absorptions of IR spectra of complexes were listed in Table 2. A comparison of the IR spectra of the complexes with that of the free ligand revealed interesting features relating to the metal-ligand interactions. The characteristic absorptions of enrofloxacin ligand from 1627 cm^{-1} to 1385 cm^{-1} bands shifted towards lower wavenumbers after coordination. Compared to the enrofloxacin ligand (ν(COOH)=1730 cm^{-1}), complex **1** displayed three characteristic bands of the asymmetric ($\nu_{as}(COO^-)$) stretching vibration at 1577, 1529 and 1485 cm^{-1}; one symmetric (ν_s (COO^-)) stretching vibration at 1380 cm^{-1}. The difference ($\Delta\nu=\nu_{as}(COO^-)-\nu_s(COO^-)$) was a useful characteristic for determining the coordination mode of the ligand. Only one $\Delta\nu$ value was 197 cm^{-1}, which indicated a monodentate coordination mode of the carboxylato group; two $\Delta\nu$ values were 149 and 105 cm^{-1}, which exhibited chelate and bridging coordination mode [15, 16]. Complex **2**

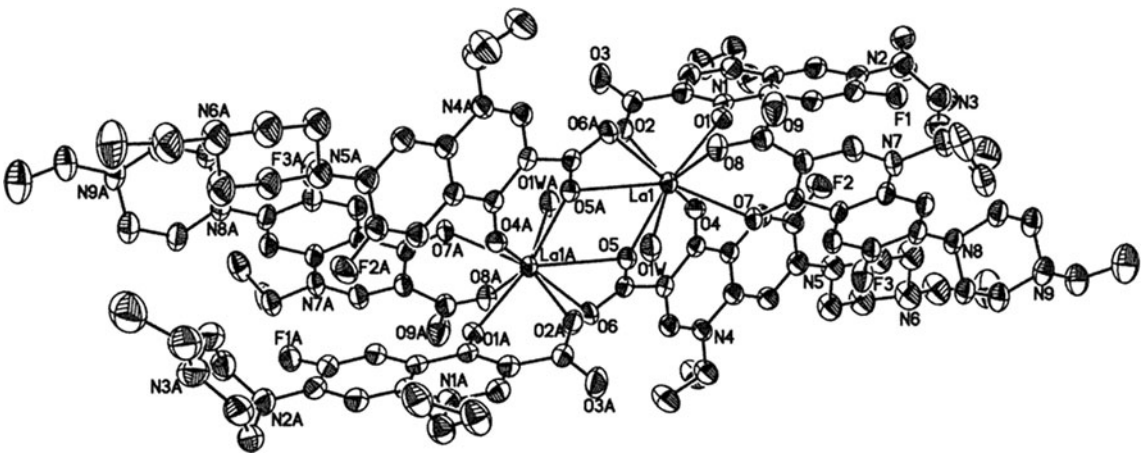

Fig. 4 Labeled ORTEP diagram of complex (**1**) with 30% thermal probability ellipsoids shown. The H atoms and lattice water molecules are omitted for clarity

Table 3 Selected bond lengths (Å) and bond angles (°) for complexes (**1**) and (**2**) with estimated standard deviations in their parentheses

Complex (1)					
Bond lengths (Å)					
La(1)-O(2)	2.468(3)	La(1)-O(1)	2.469(2)	La(1)-O(8)	2.459(3)
La(1)-O(7)	2.492(3)	La(1)-O(4)	2.552(2)	La(1)-O(5)	2.498(2)
La(1)-O(5)#1	2.716(2)	La(1)-O(6)#1	2.662(3)	La(1)-O(1 W)	2.577(3)
Bond angels (°)					
O(2)-La(1)-O(1)	68.93(9)	O(8)-La(1)-O(7)	68.35(10)	O(5)-La(1)-O(4)	66.51(7)
O(5)-La(1)-O(5)#1	63.29(12)	O(6)#1-La(1)-O(5)#1	48.24(8)	La(1)-O(5)-La(1)#1	116.71(11)
O(2)-C(3)-O(3)	123.8(4)	O(9)-C(41)-O(8)	122.9(5)	O(6)-C(22)-O(5)	121.9(3)
Complex (2)					
Bond lengths (Å)					
Sm(1)-O(2)	2.402(3)	Sm(1)-O(1)	2.4009(18)	Sm(1)-O(8)	2.426(2)
Sm(1)-O(7)	2.451(3)	Sm(1)-O(4)	2.510(2)	Sm(1)-O(5)	2.439(2)
Sm(1)-O(5)#1	2.692(2)	Sm(1)-O(6)#1	2.587(3)	Sm(1)-O(1 W)	2.477(2)
Bond angels (°)					
O(2)-Sm(1)-O(1)	73.02(8)	O(8)-Sm(1)-O(7)	69.06(9)	O(5)-Sm(1)-O(4)	67.43(6)
O(5)-Sm(1)-O(5)#1	61.58(10)	O(6)#1-Sm(1)-O(5)#1	49.39(7)	Sm(1)-O(5)-Sm(1)#1	118.42(10)
O(2)-C(3)-O(3)	121.9(3)	O(9)-C(41)-O(8)	123.8(4)	O(6)-C(22)-O(5)	121.4(3)

Symmetry transformations used to generate equivalent atoms: #1 -x,-y+2,-z+1

was similar characteristic absorptions of the carboxylato group. Furthermore, the stretching band of the $\nu(C{=}O)_{keto}$ at 1627 cm^{-1} of ligand shifted towards lower wavenumber at 1618 cm^{-1}(**1**), 1619 cm^{-1}(**2**), which illuminated the participation of the ketonic group in the bonding to the metal. In the OH stretching region, both complexes exhibited a broad band at around 3420 cm^{-1} indicative of the presence of lattice water molecules. Further, the far IR spectra of the complexes showed new bands at 496 cm^{-1}(**1**) and 501 cm^{-1}(**2**), corresponding to ν(Ln-O) vibrations. The weak bands at 540 cm^{-1}(**1**) and 551 cm^{-1}(**2**) could be assigned to the rocking vibration of water molecules, indicating the presence of coordinated water molecules.

Thermogravimetric Analysis (TGA)

The thermal decomposition of the two complexes was studied using TG-technique. The experiment was performed under a dynamic air atmosphere in the temperature range of 30 °C to 700 °C at a heating rate of 10 °C min^{-1}. It was found that the thermal behaviors of the two complexes are quite similar. We could see that the decomposition temperature of the complexes are lower than their melting points. The TG-DTG curves of complex **1** is shown in Fig. 2. According to the curves, the first weight loss of 9.26% occurring in the stages beginning at 45 °C and ending at about 118 °C corresponded to the departure of the

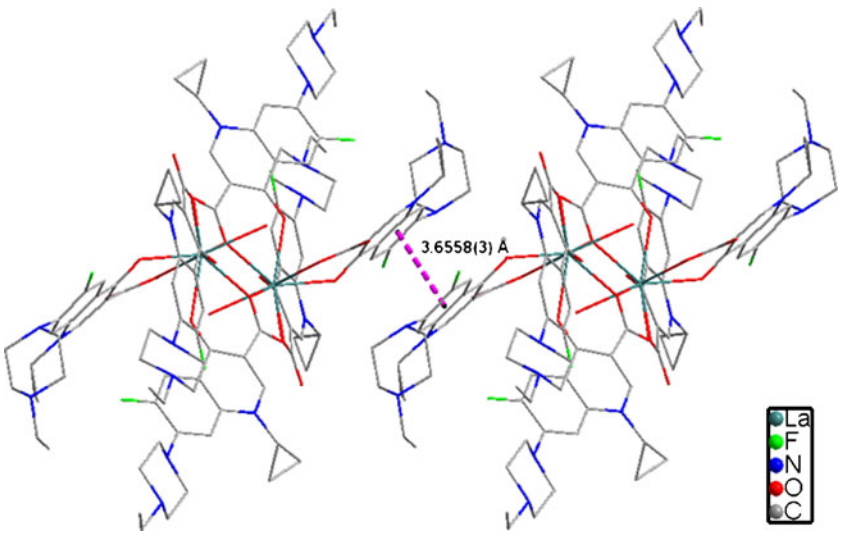

Fig. 5 π-π stacking of adjacent molecules of complex (**1**) (**a**) and complex (**2**) (**b**)

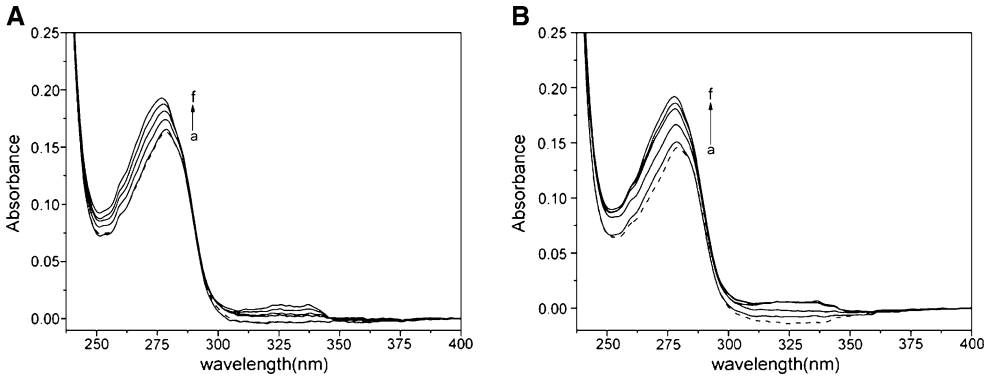

Fig. 6 Absorption spectra of BSA in the absence (*dash line*) and the presence (*solid line*) of complexes at 25 °C. **a** BSA-complex (**1**); **b** BSA-complex (**2**). c_{BSA}=4.48 μmol·L^{-1}; $c_{complex}$=0, 0.50, 1.00, 1.50, 2.00, 2.50 μmol·L^{-1}, from a to f, respectively

crystal water (calculated 9.28%). The second weight loss of 7.53% occurring in the range of 261–266 °C corresponded to the departure of the coordination water and ethyl (calculated 7.75%). Degradation of the side chain piperazinyl and fluorine atoms was observed in the range of 267–371 °C corresponding to the weight loss of 22.70% (calculated 22.78%). After that, the complex gave an endothermic peak at around 372–376 °C corresponding to the weight loss of 12.68% (calculated 12.60%), which indicates the thermal decomposition of cyclopropyl and ketone group. The last weight loss of 35.78% occurring in the range of 377–476 °C corresponded to the departure of naphthyridine and carboxylato group (calculated 35.59%). Beyond the range of 476 °C, the weight is constancy, 12.05% of the initial mass of the samples was left as a residue of La_2O_3 (calculated 12.00%).

Crystal Structure

Two new Ln(III) complexes with enrofloxacin, $[La_2(ER)_6(H_2O)_2]\cdot 14H_2O$(**1**), and $[Sm_2(ER)_6(H_2O)_2]\cdot 14H_2O$(**2**) have been characterized by X-ray single crystal diffraction. They were isostructural. The coordination model of the complexes was shown in Fig. 3. The ORTEP diagram of **1** was shown in Fig. 4.

In both complexes, each lanthanide atom was nine-coordinated; the metal environment was formed by three O_{carbox} and three O_{keto} atoms from three different enrofloxacin ligands, two carboxylate oxygen atoms from a fourth enrofloxacin ligand and one water oxygen atom in the ninth position. Two of the enrofloxacin ions acted as tridentate chelate and bridging ligands and the others as bidentate chelate ligands. In the bridging monoanions the carboxylate group behaved as a chelate ligand.

Selected bond distances and angles were listed in Table 3. For complex **1**, the La-O bond distances were in the range of 2.459(3)–2.716(2)Å for La-$O_{carbox/keto}$ and 2.577(3)Å for La-O_{water}, all of which were comparable to those reported for other La-oxygen donor complexes [17–19]. The La(1) and La(1A) atoms were linked together by sharing two edge (O(5), O(5A)) with the La···La distance of 4.4397(7) Å. For complex **2**, the Sm-O bond distances were in the range of 2.4009(18)–2.692(2)Å for Sm-$O_{carbox/keto}$ and 2.477(2)Å for Sm-O_{water}, similar to the Sm-O bond lengths in other Sm-containing polymers [20, 21]. The Sm(1) and Sm(1A) atoms were linked together by sharing two edge (O(1), O(1A)) with the Sm···Sm distance of 4.4091(6)Å.

The crystal structures were stabilized by two types of hydrogen bonds O-H···O and O-H···N for two complexes. Furthermore, weak π-π stacking was found between enrofloxacin rings with a distance of 3.6558(3)Å in the crystal packing of complex **1** (Fig. 5) and 3.6133(1)Å in complex **2**. Hydrogen bonding and weak π-π stacking formed a 3D polymeric network and stabilized the lattice structures of complex **1** and complex **2**.

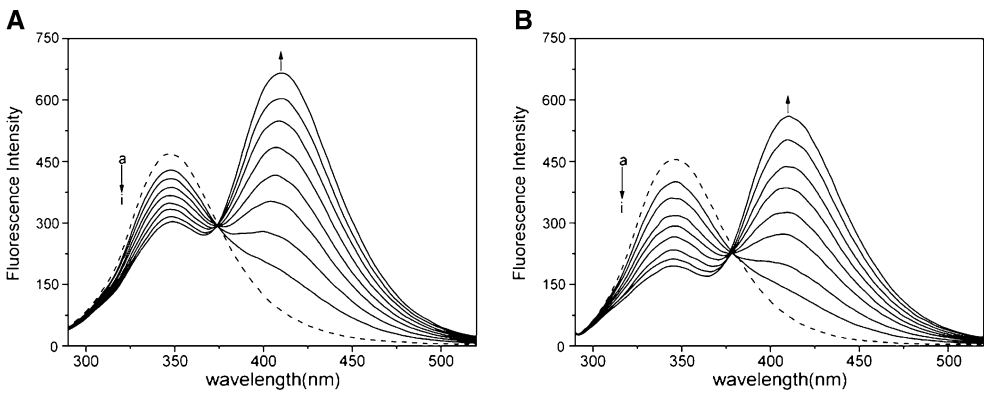

Fig. 7 Fluorescence spectra of BSA in the absence (*dash line*) and the presence (*solid line*) of complexes at 25 °C. **a** BSA-complex (**1**); **b** BSA-complex (**2**). c_{BSA}=0.50 μmol·L^{-1}; $c_{complex}$= 0, 0.08, 0.17, 0.25, 0.33, 0.42, 0.50, 0.58, 0.67 μmol·L^{-1}, from a to i, respectively

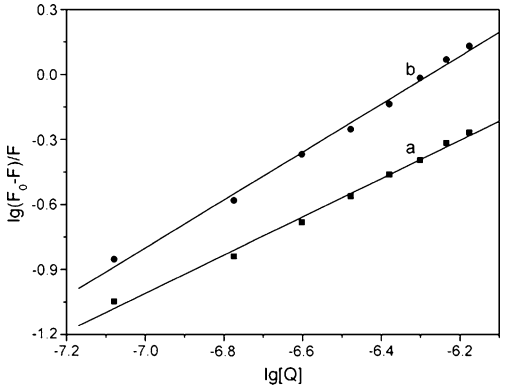

Fig. 8 Logarithmic plots of fluorescence quenching of BSA. **a** complex **1**; **b** complex **2**

Interaction with BSA

UV-vis Absorption Apectra

The UV absorption spectra of BSA was assigned to π-π* transition of aromatic amino acid residues with the maximun absorption wavelength at 278 nm [22]. The absorption peak of BSA showed an increasing and strong blue-shift on successive addition of complexes (Fig. 6). This shift indicated that an interaction occurred between ground state of BSA and complex molecules and the peptide strand extended even more, while the hydrophobicity was decreased (or became more polar) [23]. The binding interaction followed the trend: complex **2**>complex **1**.

Fluorescence Spectra and Quenching Mechanism

BSA has strong fluorescence emission with a peak at 350 nm on excitation at 280 nm. Its fluorescence intensity decreased in the presence of complexes. The maximum emission wavelengths of complexes were at 410 nm and fluorescence intensity increased in systems (Fig. 7). It showed that binding of complexes to BSA could quench the intrinsic fluorescence of BSA, whereas enhance the fluorescence of complexes. These results indicated that there were strong interactions and energy transfer between complexes and BSA [24]. However, there were equivalent emission point at 373 nm (**1**) and 377 nm (**2**) in BSA-complex systems, implying that the quenching of protein fluorescence depended on the formation of enveloped-compound of BSA and complexes [25].

Fluorescence quenching is the decrease of the quantum yield of fluorescence from a fluorophore induced by a variety of molecular interactions with quencher molecules. In order to confirm the quenching mechanism, the procedure that the fluorescence quenching data was disposed to assume to be dynamic quenching. The quenching rate constants can be calculated by the Stern-Volmer equation [26]:

$$F_0/F = 1 + K_q\tau_0[Q] \quad (1)$$

F_0 and F are the fluorescence intensities of BSA in the absence and presence of the complex, respectively. *[Q]* is

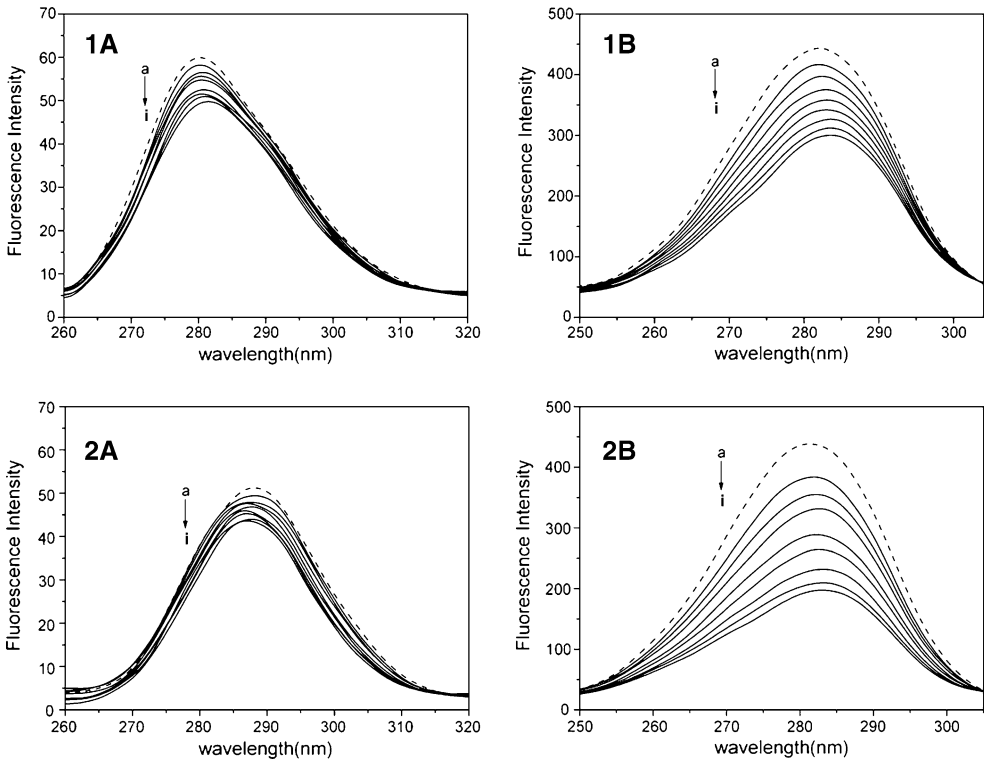

Fig. 9 Synchronous fluorescence spectra of BSA in the absence (*dash line*) and the presence (*solid line*) of complexes (**1**) and (**2**) at 25 °C. (**1**A) and (**2**A) $\Delta\lambda$=15 nm; (**1**B) and (**2**B) $\Delta\lambda$=60 nm. c_{BSA}= 0.50 μmol·L^{-1}; $c_{complex}$=0, 0.08, 0.17, 0.25, 0.33, 0.42, 0.50, 0.58, 0.67 μmol·L^{-1}, from a to i, respectively

Table 4 Relevant parameters (J, E, R_0 and r) of BSA-complexes systems

Complex	J / ($cm^3 \cdot L \cdot mol^{-1}$)	E / %	R_0 / nm	r / nm
1	2.11×10^{-13}	28.7	4.07	4.74
2	3.07×10^{-13}	49.1	4.33	4.36

the concentration of the complex. Equation 1 is applied to determine by linear fitting of a plot of F_0 / F against *[Q]*. For BSA, τ_0 (the lifetime of the fluorophore) is approximately 10^{-8} s [27]. Thus, the bimolecular quenching rate constants K_q / ($L \cdot mol^{-1} \cdot s^{-1}$) were 7.84×10^{13}(**1**) and 2.11×10^{14}(**2**), respectively. These values were much higher than the maximum value possible for diffusion-limited quenching in water (2×10^{10} $L \cdot mol^{-1} \cdot s^{-1}$), suggesting that quenching of complexes to BSA was not initiated by dynamic quenching, but static quenching from the formation of a ground-state complex between the fluorophore and quencher [28].

Binding Constants and Binding Sites Between the Complexes and BSA

Most albumins are able to associate with positively charged inorganic ions in a reversible manner. Binding of metal ions occurs at a special and well-defined binding site composed of the first three amino acids from the amino terminal end of the albumin molecule or a common series of low affinity binding sites [29].

Supposing that there are n identical and independent binding sites in protein, Eq. 2 can be obtained according to reference [30]

$$\lg(F_0 - F)/F = \lg K_A + n \lg[Q] \quad (2)$$

where K_A is binding constant and n is binding sites. Then Eq. 2 was applied to determine K_A and n by linear fitting of a plot of *lg* $(F_0$–$F)$ / F against *lg [Q]* (Fig. 8). K_A was calculated to be 1.46×10^5 $L \cdot mol^{-1}$(**1**), 8.59×10^6 $L \cdot mol^{-1}$(**2**), and n was 0.882(**1**), 1.105(**2**). The above data showed that there was a strong binding force and a binding site between the complexes and the BSA under the experiment concentration. The binding interaction followed the trend: complex **2**>complex **1**. This result was likely to the shorter Metal-O distances and stronger π-π stacking in complex **2** than those in complex **1**, which would lead to easier assess to hydrophobic pocket for complex **2** and binding to low affinity binding sites (the carboxyl groups) of BSA [31].

Effect of the Complexes on the BSA Conformation

The conformational changes of BSA were evaluated by measuring the synchronous fluorescence intensity of protein amino acid residues, both before and after the addition of complexes. In this work, synchronous fluorescence spectroscopy was used at different scanning intervals $\Delta\lambda$ ($\Delta\lambda=\lambda_{em}-\lambda_{ex}$). When $\Delta\lambda$=15 nm, the spectrum characteristic of the tyrosine residues was observed, and when $\Delta\lambda$= 60 nm, the spectrum characteristic of tryptophan residues was observed [32].

With the concentration of the BSA constant and the concentration of complexes increased by titration, the synchronous spectroscopy was scanned at $\Delta\lambda$=15 nm (Fig. 9(**1**A, **2**A)) and $\Delta\lambda$=60 nm (Fig. 9(**1**B, **2**B)). The effect of complexes on fluorescence intensity of BSA indicated that the main contribution was tryptophan residues. The emission maximum of tyrosine fluorescence was slightly red-shifted in complex **1** and blue-shifted in complex **2**. A stronger red-shift of tryptophan fluorescence was observed upon the addition of the complexes. This shift indicated the changes in the polarity around the tryptophan residues of BSA. Tryptophan residues were placed in a less hydrophobic environment and the inner hydrophobic structure of BSA disintegrated with the peptide chains extending increasingly [32].

Binding Distance Between the Donor (BSA) and the Acceptor (Complex)

According to the Förster's non-radioactive energy transfer theory [33], the efficiency of energy transfer, E, is given by:

$$E = 1 - F/F_0 = R_0^6/\left(R_0^6 + r^6\right) \quad (3)$$

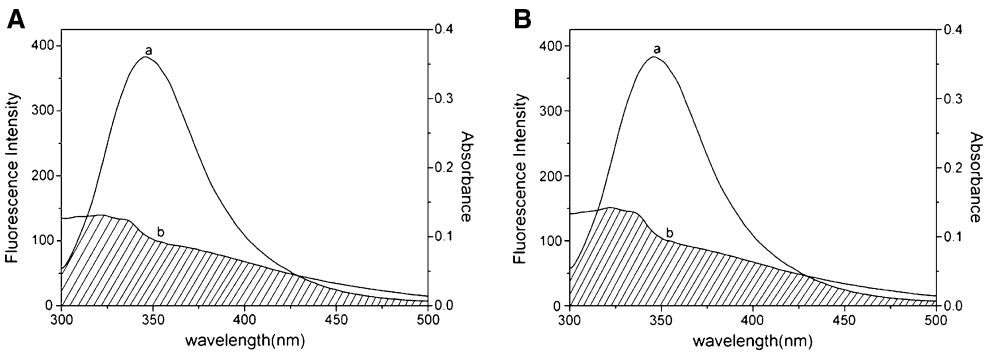

Fig. 10 Fluorescence emission spectra of BSA (**a**) and UV absorption spectra of complexes (**b**) at 25 °C. **a** compelx (**1**); **b** complex (**2**). $c_{BSA}=c_{complex}=$ 0.50 μmol·L^{-1}

where r is the donor-acceptor distance and R_0 is the distance at 50% transfer efficiency.

$$R_0^6 = 8.8 \times 10^{-25} K^2 N^{-4} \Phi J \quad (4)$$

where K^2(=2/3) is used for the dynamic averaging of the relative donor-acceptor positions in this system; N (=1.336) is the refractive index of medium, Φ (=0.118) is the fluorescence quantum yield of the donor [34] and J is the overlap integral of the fluorescence emission spectra of the donor (BSA) and the absorption spectra of the acceptor (complex). J is given by:

$$J = \left[\sum F(\lambda)\varepsilon(\lambda)\lambda^4 \Delta\lambda\right] \Big/ \left[\sum F(\lambda)\Delta\lambda\right] \quad (5)$$

where $F(\lambda)$ is the fluorescence intensity of fluorescence donor, $\varepsilon(\lambda)$ is the molar absorbance coefficient of the acceptor [35, 36]. From these relationships, the overlap integral, J, can be calculated; R_0, r and E have been listed in Table 4. The fluorescence emission spectra of BSA (a) and the absorption spectra of the complexes (b) were observed in Fig. 10(A)(**1**) and (B)(**2**), respectively .

BSA contains two tryptophan residues: Trp-134 and Trp-212. Trp-134 is located on the surface of the molecule and Trp-212 in a hydrophobic binding pocket [37]. On the experiment condition (λ_{ex}=280 nm, 298 K), it is tryptophan residue that made main contribution to the fluorescence intensity of BSA. The value of r is the distance between binding site and tryptophan residue. In Table 4, the average distance was on the 4–5 nm scale, which suggested that there was energy transfer in the binding reaction of complexes to BSA [38], while r was bigger than R_0 in the present study, and that complexes could strongly quench the intrinsic fluorescence of BSA by static quenching [39, 40].

Antibacterial Assay

Enrofloxacin, complexes **1** and **2** were assayed *in vitro* for studying their ability to inhibit the growth of representative Gram-positive (*Bacillus subtilis*, *Staphylococcus aureus*) and Gram-negative (*Escherichia coli*). DMSO was control sample. The inhibition zone diameters observed for the ligand and complexes were listed in Table 5. The data revealed that both complexes exhibited bactericidal activity. It was noteworthy that the complexes were more active than enrofloxacin at given concentrations. Hence, complexation increased the antibacterial activity, which may be due to the cooperation between enrofloxacin and rare earth ions. Furthermore, the antibacterial activity followed the trend: complex **2**>complex **1**>HER. It was likely to the structure of complex **2** was more steady and stronger interaction with BSA than complex **1**.

Table 5 The in vitro antibacterial activities of enrofloxacin and its complexes

Compounds	Diameter of inhibition zone (cm)									
	Bacillus subtilis			*Staphylococcus aureus*			*Escherichia coli*			
	0.1 mg·mL^{-1}	1.0 mg·mL^{-1}	10.0 mg·mL^{-1}	0.1 mg·mL^{-1}	1.0 mg·mL^{-1}	10.0 mg·mL^{-1}	0.1 mg·mL^{-1}	1.0 mg·mL^{-1}	10.0 mg·mL^{-1}
DMSO		0.9			1.3			1.1	
Enrofloxacin	2.4	2.8	3.0	1.7	2.5	2.7	4.4	5.0	5.8
$[La_2(ER)_6(H_2O)_2]\cdot 14H_2O$	2.3	3.6	4.2	2.6	3.2	3.5	5.0	5.3	6.5
$[Sm_2(ER)_6(H_2O)_2]\cdot 14H_2O$	2.5	3.8	4.1	2.8	3.2	3.7	5.2	5.6	6.6

Conclusion

Two new crystals of rare earth complexes with enrofloxacin $[Ln_2(C_{19}H_{21}FN_3O_3)_6(H_2O)_2]\cdot 14H_2O$, (Ln=La(III) and Sm (III)) have been obtained and determined by elemental analysis, FT-IR, TG-DTG and X-ray diffraction. In the complexes, two of the enrofloxacin ions acted as tridentate chelate and bridging ligands and the others bidentate chelate ligands. Coordination number was nine. UV-vis absorption spectra and fluorescence spectroscopy indicated that the complexes had a quite strong ability with BSA, and 1:1 enveloped-compound was formed. Quenching of complexes to BSA was mainly a static quenching process. Trytophan residue made main contribution to the fluorescence intensity of BSA. Antibacterial active results showed that the complexes exhibited greater antimicrobial activity compared to enrofloxacin. All the results could help us to understand the relation among the binding ability of the BSA-complex, the quenching mechanism and the antimicrobial activities. This will be significant for further development of quinolone drugs and improvement of medicinal value of rare earth.

Supplementary data

CCDC 738498 and 725878 contain the supplementary crystallographic data for this paper. These data can be obtained free of charge via http://www.ccdc.cam.ac.uk/conts/retrieving.html, or from the Cambridge Crystallographic Data Center, 12 Union Road, Cambridge CB2 1EZ, UK; fax: (+44) 1223-336-033; or e-mail: deposit@ccdc.cam.au.uk.

Acknowledgements This work received financial support from the Natural Science Foundation of Zhejiang Province, China (Grant No. Y407301).

References

1. Guo M, Zou JW, Yi PG, Shang ZC, Hu GX, Yu QS (2004) Binding Interaction of Gatifloxacin with Bovine Serum Albumin. Anal Sci 20:465–470
2. Wang YP, Wei YL, Dong C (2006) Study on the interaction of 3, 3-bis(4-hydroxy-1-naphthyl)-phthalide with bovine serum albumin by fluorescence spectroscopy. J Photochem Photobiol A 177:6–11
3. Flarakos J, Morand KL, Vouros P (2005) High-Throughput Solution-Based Medicinal Library Screening against Human Serum Albumin. Anal Chem 77:1345–1353
4. Pasquali F, Manfreda G (2007) Mutant prevention concentration of ciprofloxacin and enrofloxacin against *Escherichia coli*, *Salmonella* Typhimurium and *Pseudomonas aeruginosa*. Vet Microbiol 119:304–310
5. e Souza MJ, Bittencourt CF, Morsch LM (2002) LC determination of enrofloxacin. J Pharm Biomed Anal 28:1197–1199
6. Boothe DM (1994) Enrofloxacin revisited. Vet Med 89:744–753
7. e Souza MJ, Bittencourt CF, e Souza Fillho PS (2004) Microbiological assay for enrofloxacin injection. Int J Pharm 271:287–291
8. Tarushi A, Psomas G, Raptopoulou CP, Psycharis V, Kessissoglou DP (2009) Structure and DNA-binding properties of bis(quinolonato) bis(pyridine)zinc(II) complexes. Polyhedron 28:3272–3278
9. Efthimiadou EK, Katsaros N, Karaliota A, Psomas G (2007) Synthesis, characterization, antibacterial activity, and interaction with DNA of the vanadyl-enrofloxacin complex. Bioorg Med Chem Lett 17:1238–1242
10. Zhu WZ, Lin QY, Lu M, Hu RD, Zheng XL, Cheng JP, Wang YY (2009) Synthesis, Characterization, DNA-Binding and Antiproliferative Activity of Nd(III) Complexes With N-(Nitrogen Heterocyclic) Norcantharidin Acylamide Acid. J Fluoresc 19:857–866
11. Komiyama M, Takeda N, Shigekawa H (1999) Hydrolysis of DNA and RNA by lanthanide ions: mechanistic studies leading to new applications. Chem Comm 16:1443–1451
12. Zhang XJ, Xing YH, Han J, Zeng XQ, Ge MF, Niu SY (2008) A Series of Novel Ln-Succinate-Oxalate Coordination Polymers: Synthesis, Structure, Thermal Stability, and Fluorescent Properties. Cryst Growth Des 8:3680–3688
13. Sheldrick GM (1997) SHELXS 97. Program for the Solution of Crystal Structures. University of Gottingen, Germany
14. Sheldrick GM (1997) SHELXL 97. Program for the Refinement of Crystal Structures. University of Gottingen, Germany
15. Deacon GB, Phillips RJ (1980) Relationships between the carbon-oxygen stretching frequencies of carboxylato complexes and the type of carboxylate coordination. Coord Chem Rev 33:227–250
16. Zhang F, Zhang QQ, Wang WG, Wang XL (2006) Synthesis and DNA binding studies by spectroscopic and PARAFAC methods of a ternary copper(II) complex. J Photochem Photobiol A 184:241–249
17. Neogi S, Bharadwaj PK (2006) Metal-organic frameworks of lanthanide (III) ions with a podand bearing terminal carboxylates: Identification of water clusters of different nuclearity. Polyhedron 25:1491–1497
18. Thirumurugan A, Natarajan S (2005) Hydrothermal synthesis, structure and luminescent properties of one-dimensional lanthanide benzenedicarboxylates, $[M(NO_3)M_2(C_{12}H_8N_2)_2][(C_8H_4O_4)_4]\cdot H_2O$, (M=La, Pr), possessing infinite M–O–M linkages. J Mater Chem 15:4588–4594
19. Hu DX, Luo F, Che YX, Zheng JM (2007) Construction of Lanthanide Metal—Organic Frameworks by Flexible Aliphatic Dicarboxylate Ligands Plus a Rigid *m*-Phthalic Acid Ligand. Cryst Growth Des 7:1733–1737
20. Zhang GQ, Yang GQ, Ma JS (2006) Hydrothermal Syntheses and Characterization of Novel 3D Open-Framework and 2D Grid Lanthanide Fumarates: $Ln_2(fum)_3(H_2fum)(H_2O)_2$ (Ln=Ce or Nd), $[Sm_2(fum)_3(H_2O)_4](H_2O)_3$, and $[Yb_2(fum)_3(H_2O)_4](H_2O)_2$. Cryst Growth Des 6:933–939
21. Song YS, Yan B, Weng LH (2007) Four distinctive 1-D lanthanide carboxylate coordination polymers: Synthesis, crystal structures and spectral properties. Polyhedron 26:4591–4601
22. Shen XC, Yuan Q, Liang H, Yan HG, He XW (2003) Hysteresis effects of the interaction between serum albumins and silver nanoparticles. Sci China B 46:387–398
23. Hu YJ, Liu Y, Pi ZB, Qu SS (2005) Interaction of cromolyn sodium with human serum albumin: A fluorescence quenching study. Bioorg Med Chem 13:6609–6614
24. Ashoka S, Seetharamappa J, Kandagal PB, Shaikh SMT (2006) Investigation of the interaction between trazodone hydrochloride and bovine serum albumin. J Lumin 121:179–186
25. Xiao JB, Wei XL, Wang YF, Liu CX (2009) Fluorescence resonance energy-transfer affects the determination of the affinity between ligand and proteins obtained by fluorescence quenching method. Spectrochim Acta A 74:977–982

26. Lakow JR, Weber G (1973) Quenching of Fluorescence by Oxygen. A Probe for Structural Fluctuations in Macromolecules. Biochem 12:4161–4170
27. Jiang CQ, Gao MX, He JX (2002) Study of the interaction between terazosin and serum albumin Synchronous fluorescence determination of terazosin. Anal Chim Acta 452:185–189
28. Li GZ, Liu YM, Guo XY, Wang JJ (2006) Study on the Interaction between Bovine Serum Albumins and Topotecan Hydrochloride or I rinotecan Hydrochloride. Acta Chim Sinica 64:679–685
29. Kragh-Hansen U (1981) Molecular Aspects of Ligand Binding to Serum Albumin. Pharmacol Rev 33:17–53
30. Xie MX, Xu XY, Wang YD, Liu Y (2005) Spectroscopic Investigation of the Interaction between 2, 3-Dihydro-4', 5, 7-trihydroxyflavone and Human Serum Albumin. Acta Chim Sinica 63:2055–2062
31. Kang YZ, Shen HB, Luo YQ, Yang HF, Shao L (2002) Spectral Study on the Interaction of Rare Earth Ions with BSA. Chin Rare Earths chinese 23:22–25
32. Wang CX, Yan FF, Zhang YX, Ye L (2007) Spectroscopic investigation of the interaction between rifabutin and bovine serum albumin. J Photochem Photobiol A 192:23–28
33. Förster T, Sinanoglu O (1996) Modern quantum chemistry, vol 3. Academic, New York
34. Yang J, Jing ZH, Jie JJ, Guo P (2009) Fluorescence spectroscopy study on the interaction between Gossypol and bovine serum albumin. J Mol Struct 920:227–230
35. Liu JQ, Tian JN, Zhang JY, Hu ZD, Chen XG (2003) Interaction of magnolol with bovine serum albumin: a fluorescence-quenching study. Anal Bioanal Chem 376:864–867
36. Zhang ZQ, Liang GX (2005) Flow injection on-line oxidizing fluorometry coupled to dialysis sampling for the study of carbamazepine–protein binding. Anal Chim Acta 536:145–151
37. Peters T (1985) Serum albumin. Adv Protein Chem 37:161–245
38. Zhang GW, Wang AP, Jiang T, Guo JB (2008) Interaction of the irisflorentin with bovine serum albumin: A fluorescence quenching study. J Mol Struct 891:93–97
39. He W, Li Y, Xue C, Hu Z, Chen XG, Sheng FL (2005) Effect of Chinese medicine alpinetin on the structure of human serum albumin. Bioorg Med Chem 13:1837–1845
40. Wang YQ, Zhang HM, Zhang GC, Zhou QH, Fei ZH, Liu ZT, Li ZX (2008) Fluorescence spectroscopic investigation of the interaction between benzidine and bovine hemoglobin. J Mol Struct 886:77–84